

# Enhancing Long-distance Continuous-variable Quantum-key-distribution with an Error-correcting Relay

S. Nibedita Swain,<sup>1, 2, 3,\*</sup> Ryan J. Marshman,<sup>3</sup> Josephine Dias,<sup>3</sup> Alexander S. Solntsev,<sup>1</sup> and Timothy C. Ralph<sup>3</sup>

<sup>1</sup>*School of Mathematical and Physical Sciences, University of Technology Sydney, Ultimo, NSW 2007, Australia*

<sup>2</sup>*Sydney Quantum Academy, Sydney, NSW 2000, Australia*

<sup>3</sup>*Centre for Quantum Computation and Communication Technology,  
School of Mathematics and Physics, University of Queensland, Brisbane, Queensland 4072, Australia*

(Dated: December 15, 2025)

Noiseless linear amplifiers (NLAs) serve as an effective means to enable long-distance continuous-variable (CV) quantum key distribution (QKD), even under realistic conditions with non-unit reconciliation efficiency. Separately, unitary averaging has been suggested to mitigate some stochastic noise, including phase noise in continuous-variable states. In this work, we combine these two protocols to simultaneously compensate for thermal-loss effects and suppress phase noise, thereby enabling long-distance CV QKD that surpasses the repeaterless bound, the fundamental rate-distance limit, for repeaterless quantum communication systems.

## I. INTRODUCTION

Quantum Key Distribution (QKD) enables the creation of a shared, secure key between a sender and a receiver, even when communication occurs over an untrusted channel that may be entirely controlled by an eavesdropper. Within this context, continuous-variable (CV) QKD has emerged as a particularly promising approach, both from theoretical and experimental perspectives [1]. In CV QKD schemes [2–5], the sender (Alice) encodes information onto the quadratures of a optical field using Gaussian modulation, which is subsequently transmitted through a channel to the receiver (Bob). Bob then performs either homodyne or heterodyne (double-homodyne) measurements [6]. The secure key is derived following a reconciliation procedure in which one of the communicating parties raw key is treated as the correct key: direct reconciliation [7] for Alice’s key, and reverse reconciliation if it is Bob’s key. Using reverse reconciliation allows a non-zero secure key rate for any transmission distance in the asymptotic limit of a pure-loss channel [8, 9].

In practical scenarios, the secret key rate (SKR), defined as the length of the secret key shared between Alice and Bob per use of the quantum channel, is significantly influenced not only by loss and thermal noise but also by phase noise. These factors severely impact the achievable SKR and limit the maximum transmission distance at which the SKR ultimately vanishes. Whilst thermal-loss channels have long been analysed, a recent study by Kish et al., demonstrated that phase noise notably degrades the performance of CV-QKD systems [10]. Here, we propose to address these challenges by modifying the original protocol by introducing strategies that effectively mitigate phase noise and thermal loss in order to extend the maximum possible transmission distance. Two promising techniques in this regard are unitary averaging (UA)

[11, 12] and heralded noiseless linear amplification (NLA) [13–16], both of which offer intriguing avenues to enhance the robustness and range of CV-QKD implementations.

UA is a framework that has been predicted to be effective in mitigating phase errors in CV linear optical systems [12] albeit at the cost of making the channel probabilistic. In such setups, each input state is simultaneously sent through multiple copies of the transmission channel before being recombined with vacuum heralding of the non-output channels. Previous results [12] have indicated this process provides substantial benefits in protecting Gaussian states against phase errors. Notably, the robustness of this protocol persists even in the presence of losses within the optical components.

An ideal probabilistic NLA with amplitude gain  $g$  can extend the maximum transmission distance in proportion to  $\log g$  [17]. However, any physically realizable NLA can only approximate the ideal performance for optical signals with low amplitudes. Recently, CV QKD schemes employing Quantum Scissors (QS) [18] to act as a Noiseless Linear Amplifier (NLA) have been investigated, enabling long-distance CV-QKD under conditions of sufficiently low channel excess noise [19]. Winnel et al., demonstrated that QS devices can function as loss-tolerant quantum relays by themselves, simultaneously performing entanglement distillation and entanglement swapping with a distributed NLA. Consequently, the repeaterless, or Pirandola–Laurenza–Ottaviani–Banchi (PLOB), bound [20] can be surpassed without the need for quantum memories [21].

In this work, we first demonstrate that, despite its probabilistic nature, UA can increase the transmission distance of CV-QKD in the presence of phase-noise. We then study how it can be successfully combined with a distributed NLA relay scheme. The first half of the article focuses on modelling phase noise within the entanglement-based (EB) version of the CV-QKD protocol and implement the UA protocol, demonstrating improvements in secret key rates. In the second half, we consider the effect of thermal loss and phase noise on the per-

\* [swain.nibedita@gmail.com](mailto:swain.nibedita@gmail.com)

formance of an NLA based repeater set-up. We then combine UA an NLA, forming a hybrid protocol capable of surpassing the PLOB bound and enabling long-distance CV-QKD even in the presence of substantial noises.

The structure of this paper is as follows. Section II reviews no switching CV-QKD protocol we will be using. Section III presents how phase noise constrains the transmission distance and then introduces the UA-assisted CV-QKD protocol. In Section IV, we first discuss the impact of phase noise in the relay-based scheme, after which we present the hybrid UA–NLA protocol, including a comparison of the SKRs of the protocols considered. Finally, Section V summarizes our results and offers concluding remarks.

## II. THE CV QKD PROTOCOL

We begin by reviewing the no switching CV-QKD protocol used throughout this work, focusing on its entanglement-based version, which allows for a more straightforward theoretical study [7]. In this framework, Alice initially creates a two-mode squeezed vacuum (TMSV) state, given by  $|\text{TMSV}\rangle = (\cosh r)^{-1} \sum_{n=0}^{\infty} (-\tanh r)^n |n, n\rangle$ . The TMSV is a two-mode Gaussian state [1, 22], which can be fully characterized by its covariance matrix (CM) (see Appendix B for additional details):

$$\Sigma_{\text{TMSV}} = \begin{pmatrix} \mathbb{A}\mathbf{I}_2 & \mathbb{C}\sigma_2 \\ \mathbb{C}\sigma_2 & \mathbb{B}\mathbf{I}_2 \end{pmatrix}, \quad (1)$$

where  $\mathbb{A} = \mathbb{B} = \cosh 2r$  corresponding to the input modulation variance of the protocol, denotes the TMSV variance.  $\mathbb{C} = \sinh 2r$ ,  $\mathbf{I}_2 = \text{diag}(1, 1)$ , and  $\sigma_2$  represents the Pauli  $z$  matrix. All variables are expressed in shot-noise units.

Alice carries out a heterodyne measurement on one mode, while the second mode is transmitted to Bob through an untrusted quantum channel, modelled as a thermal-loss channel. The channel is characterized by a transmissivity given by  $\eta = 10^{-L/10D}$ , where  $D$  denotes the transmission distance in kilometers, and  $L \sim 0.2$  dB/km represents the typical loss coefficient for optical fibers operating at 1550 nm [23, 24].

Furthermore, the presence of excess noise  $\epsilon$ , which may arise due to various imperfections, is modeled by a single-mode thermal bath containing  $n_{\text{th}} = \eta\epsilon/2(1 - \eta)$  photons [9]. The losses and imperfections impact the signal received by Bob, which experiences an added noise  $\varkappa = (1 - \eta)/\eta + \epsilon$ , resulting in an overall thermal-loss channel. Consequently, the quantum state shared between Alice and Bob remains Gaussian, characterized by the covariance matrix (CM) [6, 25, 26].

$$\Sigma_{\text{AB}}^{(\text{Th})} = \begin{pmatrix} \Sigma_A & \Sigma_C \\ \Sigma_C & \Sigma_B \end{pmatrix}, \quad (2)$$

$$= \begin{pmatrix} \mathbb{A}\mathbf{I}_2 & \sqrt{\eta}\mathbb{C}\sigma_2 \\ \sqrt{\eta}\mathbb{C}\sigma_2 & \eta(\mathbb{A} + \varkappa)\mathbf{I}_2 \end{pmatrix}. \quad (3)$$

Upon receiving the signal, Bob performs a Gaussian measurement [27] of a quadrature randomly selected between  $q$  and  $p$ , as in the original protocol [28].

All the necessary information to perform the security analysis is contained in the covariance matrix (3). According to the Gaussian formalism [4, 26, 28], when Alice and Bob perform detection on their own signals they get a bivariate Gaussian distribution with zero mean and covariance  $\Sigma_B + \Lambda_B^{(\text{m})}$ , where

$$\Lambda_B^{(\text{m})} = \lim_{\sigma \rightarrow \infty} \begin{pmatrix} \sigma & 0 \\ 0 & \sigma^{-1} \end{pmatrix} \quad (4)$$

$\Lambda_B^{(\text{m})}$  is the CM with the homodyne detection. Sifting can be relevant for systems based on homodyne detection or squeezed states, as only a single quadrature may be accessed in each measurement. The mutual information between Alice and Bob is then given by

$$I_{\text{AB}} = H(A) + H(B) - H(AB) \quad (5)$$

$$= \log_2 \sqrt{\frac{\det(\Sigma_A + \Lambda_A^{(\text{m})}) \det(\Sigma_B + \Lambda_B^{(\text{m})})}{\det(\Sigma_{\text{AB}} + (\Lambda_A^{(\text{m})} \oplus \Lambda_B^{(\text{m})}))}}, \quad (6)$$

where  $H(x) = -\int p(x) \log_2 p(x) dx$  or  $H(x) = -\sum_x p(x) \log_2 p(x)$  is the Shannon entropy of  $p(x)$ .

Throughout this paper we concentrate on a reverse reconciliation scheme, which has been shown to provide stronger security than direct reconciliation [29, 30]. We also assume the eavesdropper (Eve) can perform collective attacks, which constitute the most powerful attacks available to them in the asymptotic limit of an infinite data set [5]. The SKR in the asymptotic limit is

$$\kappa = \beta I_{\text{AB}} - \chi_{\text{BE}}, \quad 0 \leq \beta \leq 1 \quad (7)$$

where  $\beta$  is the reconciliation efficiency and the Holevo information,  $\chi_{\text{BE}}$ , quantifies the amount of information that Eve can extract [31]. This can be calculated from the covariance matrix (CM) (3) as

$$\chi_{\text{BE}} = G\left(\frac{g_1 - 1}{2}\right) + G\left(\frac{g_2 - 1}{2}\right) - G\left(\frac{g_3 - 1}{2}\right) \quad (8)$$

where

$$G(x) = (x + 1) \log_2(x + 1) - x \log_2 x \quad (9)$$

$g_{1(2)}$  are the symplectic eigenvalues of  $\Sigma_{\text{AB}}$  [1, 26]. The above estimation is derived under the assumption of infinitely large modulation and detection data. In practical

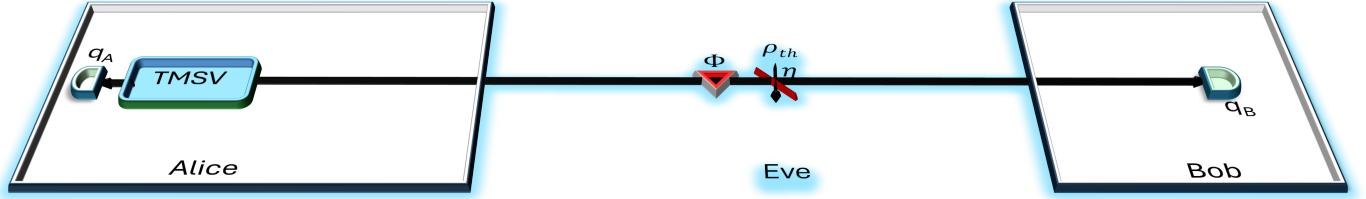


Figure 1: The squeezed-state protocol is subjected to the phase ( $\phi$ ) and thermal ( $\rho_{th}$ ) noise channel. TMSV denotes the two-mode squeezed vacuum state.

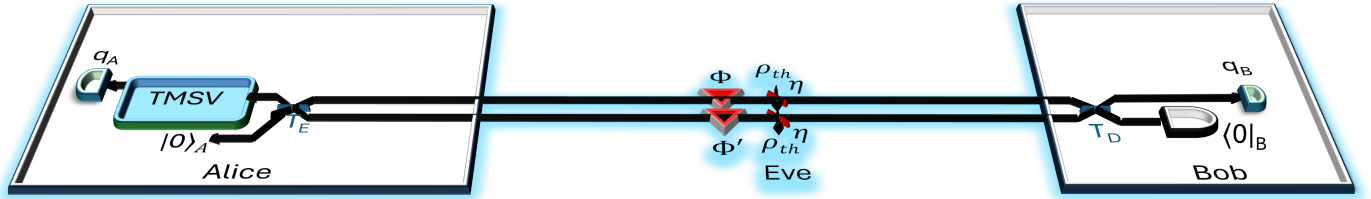


Figure 2: The squeezed-state protocol is illustrated incorporating the UA scheme. The elements  $T_E$  and  $T_D$  denote the 50:50 beamsplitters used for encoding and decoding, respectively. The term  $\langle 0|_B$  represents the vacuum detection performed by Bob.

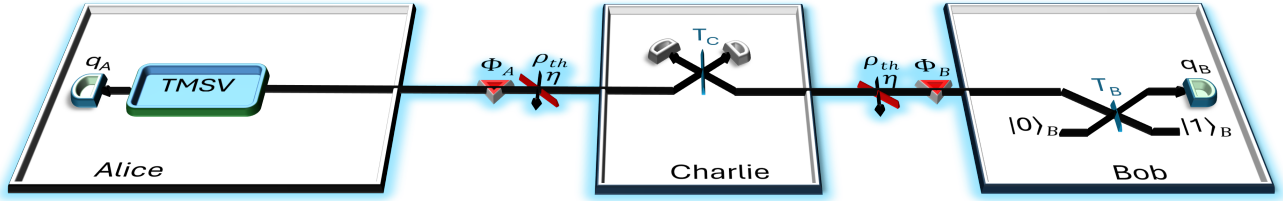


Figure 3: CV-QKD protocol for overcoming the PLOB bound along with the phase noise. Alice selects one mode from the TMSV state and transmits it to Charlie through a channel affected by both thermal noise and phase noise. Simultaneously, Bob generates a single-photon entangled state and directs one of its modes toward Charlie as well.

Upon receiving the modes, Charlie interferes them using a 50:50 beamsplitter and performs photon-number-resolving detection. A single detection event (click) signifies the presence of strong correlations between Alice and Bob. Subsequently, Bob measures his remaining mode via heterodyne detection. The gain of the NLA is adjusted according to Charlie's precise position between Alice and Bob, as well as the transmissivities of the beamsplitters,  $T_C$  and  $T_B$ .

CV-QKD systems, however, the data length is necessarily finite, which introduces statistical fluctuations in the estimated parameters. Despite these finite-size effects, the asymptotic key rate remains a benchmark for validating the feasibility of the proposed scheme and for guiding experimental design.

In the following, we investigate how the simultaneous presence of phase noise, pure loss and thermal noise affect the channel (see Fig. 1 for set-up), and we analyse the resulting key rate,  $\kappa$ , as a function of the transmission distance under these noise conditions. We then study the behaviour of  $\kappa$  as a function of the transmission distance for the UA-assisted protocol (Fig. 2) in Section III. Subsequently, we incorporate phase noise into the relay scheme once again (Fig. 3). Finally, we apply the hybrid

UA-NLA protocol and study the behaviour of  $\kappa$  as a function of the transmission distance under these noise conditions, following the scheme described in Section IV.

Throughout the analysis, we assume a fixed reconciliation efficiency of  $\beta \sim 0.95$  and an excess noise  $\epsilon = 0.02$  [32]. The excess noise is taken to originate from the environment and is modelled as input thermal noise.

### III. UA-ASSISTED CV QKD

In this section, we begin by considering a scenario in which Alice prepares a TMSV state and sends one of its modes through both a phase-noise channel and a thermal-loss channel, as illustrated in Fig. 1. The phase

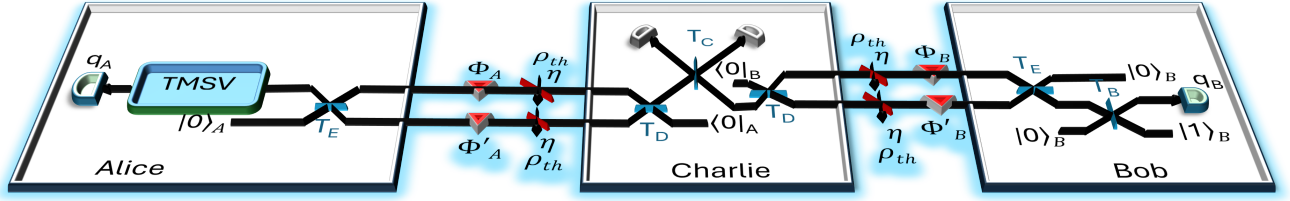


Figure 4: CV-QKD protocol for overcoming the PLOB bound with UA scheme. Alice prepares a TMSV state along with a vacuum state. After completing the encoding step using a 50:50 beamsplitter, she sends both modes to Charlie’s station. In parallel, Bob prepares a single-photon entangled state together with a vacuum state. Similarly, after performing the encoding step, Bob sends both modes to Charlie’s station. At Charlie’s end, the decoding step is carried out using a 50:50 beamsplitter for both Alice and Bob. Upon successful heralding on the vacuum outcomes for the respective vacuum modes of Alice and Bob, Charlie interferes the remaining modes using a 50:50 beamsplitter and performs photon-number-resolving detection.

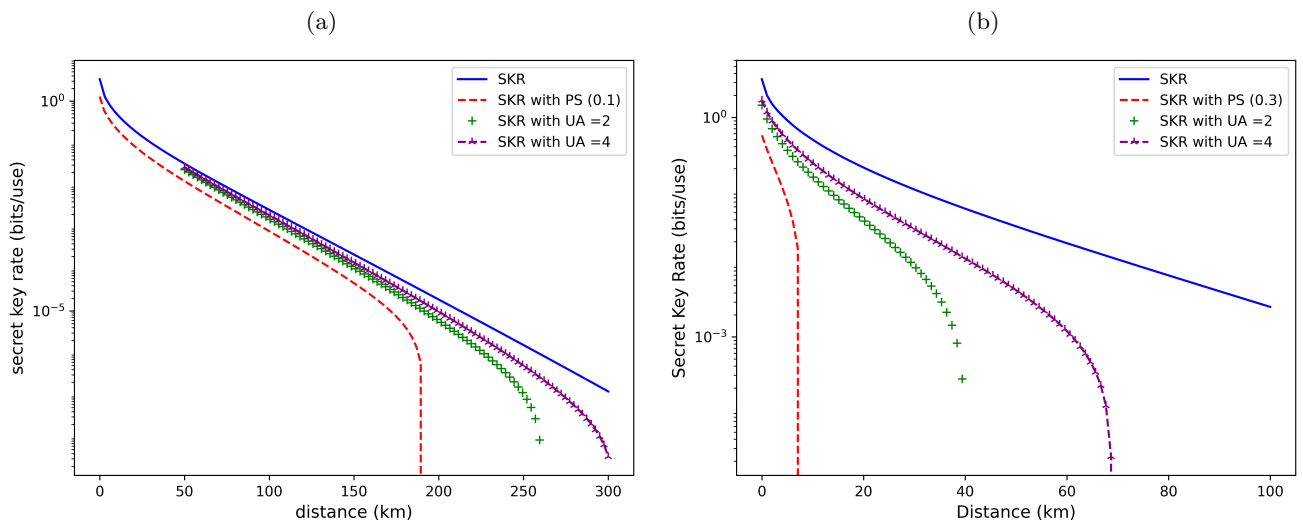


Figure 5: Secret key rate as a function of transmission distance in with  $\beta = 0.95$  and excess noise  $\epsilon = 0.02$ . The solid blue line represents the case without phase noise. 5a and 5b represent SKR with phase noise  $\sigma = 0.1$  and  $\sigma = 0.3$  respectively. In the both the plots, the dashed, red line represents SKR with phase noise. The Green line with marker ‘+’ and purple dashed-+ line clearly shows the improvement after applying the UA protocol once ( $N = 2$ ) and twice ( $N = 4$ ) respectively.

noise in this setup is modelled by fluctuations in the phase shifter (PS) parameters, drawn from independent Gaussian distributions for each mode. Physically, this could arise from small, independent fluctuations in path distance with respect to the local oscillator.

Next, we present the UA protocol, illustrated in Fig. 2. In this protocol, Alice, in addition to preparing the TMSV state, also generates an auxiliary mode in the vacuum state. Subsequently, Alice combines the second mode of the TMSV state with the vacuum state using an encoding beamsplitter ( $T_E$  in Fig. 2), which is a 50:50 beamsplitter. The dual mode signal then propagates through the thermal loss and phase noise channel before being recombined by Bob using the decoding beamsplitter ( $T_D$  in Fig. 2). It is assumed that the phase noises affecting the two-modes are of equal magnitude,

but are independent. Finally, Bob performs vacuum detection on the vacuum mode. After performing a Gaussian measurement on the other mode, Bob obtains the phase-reduced state.

As discussed in [12], the resulting output state is approximately Gaussian. Consequently, the protocol depicted in Figs. (1, 2) is equivalent to the scheme described in Section II. Thus, in our approach, it is sufficient to compute the covariance matrices (CMs)  $\Sigma_{AB}^{(\text{PS})}$  and  $\Sigma_{AB}^{(\text{UA})}$ , corresponding to the states  $\rho_{\text{PS}}$  and  $\rho_{\text{UA}}$ , respectively, in order to carry out the security analysis. These CMs can

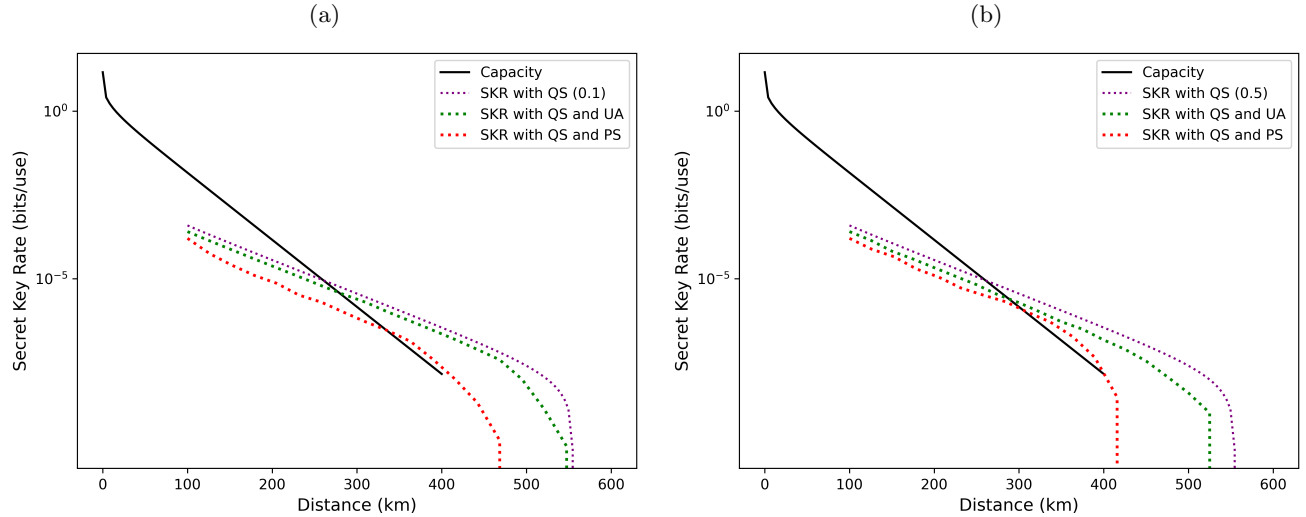


Figure 6: SKRs as functions of the distance in kilometers with  $\beta = 0.95$  and excess noise  $\epsilon = 0.02$  with and without applying hybrid UA-NLA protocol. 6a and 6b represent SKR with phase noise  $\sigma = 0.1$  and  $\sigma = 0.5$  respectively. In the both the plots, red dotted line represents SKR with phase noise when employing the distributed NLA protocol. The green dotted line clearly shows the improvement after applying the hybrid UA-NLA protocol. The purple dotted line in both the plots show the keyrate with an NLA but no phase noise.

be written

$$\Sigma_{AB}^{(PS)} = \begin{pmatrix} A_{PS} \mathbf{I}_2 & C_{PS} \sigma_2 \\ C_{PS} \sigma_2 & B_{PS} \mathbf{I}_2 \end{pmatrix} \quad (10)$$

$$\Sigma_{a1b1}^{(UA)} = \begin{pmatrix} A_{UA} \mathbf{I}_2 & C_{UA} \sigma_2 \\ C_{UA} \sigma_2 & B_{UA} \mathbf{I}_2 \end{pmatrix} \quad (11)$$

The expressions for  $\Sigma_{AB}^{(PS)}$  and  $\Sigma_{a1b1}^{(UA)}$  are provided in Appendix C. The detailed derivations, including the explanation of the Kraus operator representation, are provided in Appendix C. We evaluate the mutual information and the Holevo information following the procedure outlined in Section II, by substituting  $\rho_{AB} \rightarrow \rho_{AB}^p$  with  $p = (\text{PS}, \text{UA})$ , and then use Eq. 7 to compute the corresponding SKRs.

$$\kappa^{(\text{PS})} = \beta I_{AB}^{(\text{PS})} - \chi_{\text{BE}}^{(\text{PS})} \quad (12)$$

$$\kappa^{(\text{UA})} = P^{(\text{UA})} (\beta I_{AB}^{(\text{UA})} - \chi_{\text{BE}}^{(\text{UA})}) \quad (13)$$

$\kappa^{(\text{UA})}$  is defined as the raw key rate multiplied by the success probability of the UA protocol, denoted by  $P^{(\text{UA})}$ . Both  $\kappa^{(\text{PS})}$  and  $\kappa^{(\text{UA})}$  correspond to the asymptotic secret key rates without and with the application of the UA protocol, respectively. A detailed explanation of the UA protocol is provided in Appendix A. The procedure for applying the UA protocol once is given in Appendix C3. To apply the protocol twice, the input state is combined with two ancilla modes using (50:50) beam-splitters as per the encoding step. Each mode then undergoes identical and independent phase noise. The decoding beam splitter network subsequently reverses the encoding.

After heralding vacuum in the two auxiliary modes, the resulting output state exhibits improved quality. The corresponding calculations for the double application of the UA protocol can be carried out by following the methods presented in Appendices A and C3.

Next, we compare the SKRs obtained with and without applying the UA protocol. The red dashed lines in Fig. 5 illustrate that phase noise significantly limits the transmission distance compared with the solid black line, which represents the case without phase noise. In Fig. 5a, for a phase-noise channel with  $\sigma = 0.1$  and a thermal-loss channel characterized by an excess noise of  $\epsilon = 0.02$ , the SKR without UA drops to zero around 190 km. However, with the application of UA, the key rate extends up to approximately 300 km, indicating an improvement of about 110 km. Similarly, in Fig. 5b, for a higher phase noise of  $\sigma = 0.3$ , the asymptotic key rate without UA vanishes around 5 km. In contrast, applying the UA protocol twice extends the key rate up to nearly 70 km.

Overall, the UA protocol demonstrates significantly enhanced performance in a decent phase-noise regime. In the following, we first discuss the NLA protocol. We then describe the how the NLA protocol is effected by the presence of phase noise. Finally, we combine the UA and NLA protocols to investigate the resulting secret key rates under conditions of phase noise.

#### IV. HYBRID UA-NLA CVQKD

Generalised quantum scissors [18, 33, 34] enable noiseless linear amplification (or deamplification) of arbitrary

input states up to a specified Fock number ( $k$ ). The operation involves combining the input state with an entanglement resource state and post-selecting on events where ( $k$ ) detectors each register a single click. This process effectively teleports and amplifies the input state onto the output mode. If the measurement and output mode are in different places, it becomes a teleamplifier. In the  $k = 1$  case, gain is determined by the transmissivity of Bob's beam splitter. When the measurement is positioned midway between Alice and Bob, the success probability of the teleamplifier scales as the square root of the total channel transmissivity. Consequently, the protocol can surpass the PLOB bound, which itself scales linearly with the total channel transmissivity; a result previously reported in [21, 34].

We consider a scenario analogous to Fig. (1b) in Ref. [21], with the addition of phase noise (Fig. 3). Alice prepares an EPR state, performs heterodyne detection, and then sends one of her modes to Charlie through a channel affected by both thermal noise and phase noise. In parallel, Bob prepares a single-photon entangled state and transmits one of its modes to Charlie. At Charlie's station, the incoming modes are interfered and measured using photon-number-resolving detectors. A single-photon detection event heralds strong correlations between Alice and Bob. Bob then heterodynes his remaining mode. The overall success probability scales with the square root of the channel transmissivity, indicating that the teleamplifier enhances the rate-distance scaling. The red dotted curves in Fig. 6 illustrate the impact of phase noise on the distributed NLA protocol.

We introduce a hybrid approach that combines the UA and distributed NLA protocols to enable long-distance CV-QKD, simultaneously mitigating phase noise and loss, allowing a positive key rate at distances surpassing the PLOB bound. In this scheme, Alice prepares a TMSV state along with an auxiliary vacuum state. After the encoding step, she transmits both entangled modes to Charlie through a thermal-noise channel and a phase-noise channel. In parallel, Bob prepares a single-photon entangled state accompanied by a vacuum state. Following his own encoding step, Bob sends the encoded modes to Charlie as well. Alice retains mode  $a_1$ , while Bob keeps mode  $b_2$ .

At Charlie's station, the decoding operation and vacuum detection for both Alice's and Bob's modes are performed. The modes ( $a_2$  and  $b_1$ ) are then interfered, and photon-number-resolving detection is carried out. A single detection click heralds enhanced correlations between Alice and Bob. The success probability scales with the square root of the overall channel transmissivity, making the teleamplifier effective in enhancing the rate-distance scaling. The gain of the NLA is determined by Charlie's position between Alice and Bob, as well as by the transmissivities of the beam splitters. A schematic illustration of the setup is provided in Figs. (3, 4). Comprehensive analytical derivations and numerical simulations supporting this scheme are presented in Appendix C4.

The corresponding secret key rates (SKRs) are computed using Eq. 7.

$$\kappa^{(\text{QS})} = P^{(\text{QS})} P^{(\text{UA})} \left( \beta I_{\text{AB}}^{(\text{QS})} - \chi_{\text{BE}}^{(\text{QS})} \right) \quad (14)$$

With the absence of UA, SKR is,

$$\kappa^{(\text{QS})} = P^{(\text{QS})} \left( \beta I_{\text{AB}}^{(\text{QS})} - \chi_{\text{BE}}^{(\text{QS})} \right) \quad (15)$$

where  $P^{(\text{QS})}$  is the total success probability where  $P^{(\text{QS})} = 2 \text{Tr} \left( (\mathbf{I}_{a1} \otimes |0\rangle \langle 0| \otimes |1\rangle \langle 1| \otimes \mathbf{I}_{b2}) \rho_{\text{AB}} \right)$ . The factor of 2 arises because there are two successful click patterns; one pattern imparts a passive  $\pi$ -phase shift on the output state, which is straightforward to correct once Charlie informs Bob which detector clicked. The success probability of the UA protocol is denoted by  $P^{(\text{UA})}$ . The PLOB bound is also shown which is  $-\log_2(1 - \eta_{\text{PLOB}})$  [20] where  $\eta_{\text{PLOB}} = 10^{-L/10D}$ ,  $D$  is the distance in km.

Figures 5 and 6 demonstrate the improvements to key rates when utilising UA without and with the distributed NLA repeater respectively. They demonstrate that even with and without phase noise and demonstrating the advantage of UA. This shows that even for moderate phase noise ( $\sigma = 0.1$  for Figures 5a and 6a) a notable improvement in key rate is achievable when utilising UA, with the maximum transmission distance improving from  $\sim 190$  km to  $> 500$  km when utilising the full UA-NLA protocol. More dramatic improvements can be seen in the higher phase noise regime, where similar transmission distances can be achieved for  $\sigma = 0.5$  with the new protocol despite a maximum transmission distance of  $< 10$  km for  $\sigma = 0.3$  for the standard no switching protocol. This protocol is tolerant to excess noise, phase noise and loss, and suggests it could improve the scaling of many recent CV QKD protocols. Of particular note is that it proves to be particularly powerful in the presence of a high phase noise channel.

## V. CONCLUSION

In this manuscript, we have investigated the use of UA to enable long-distance CV QKD under realistic conditions, and in particular demonstrated its power when combined with the distributed NLA repeater. These benefits are maintained despite non-unit reconciliation efficiency, non-zero excess channel noise, and non-zero phase noise. We propose a practical CV quantum communication protocol based on a unitary averaging techniques previously employed to mitigate phase noise and quantum scissor, which, when applied to CV QKD in the Charlie's station, surpasses the PLOB bound without requiring quantum memories, even in the presence of significant phase noise. The normalisation constant of the output state after the vacuum detection yeilds the success probability of UA, which was found to be sufficiently high with the noise channels considered. When the station is

placed symmetrically between Alice and Bob with balanced beamsplitters, the NLA success probability scales as  $\sqrt{n}$ , and the NLA gain across the second link compensates for the loss in the first link. Consequently, the UA-NLA protocol protects against both phase noise and loss, and is robust to thermal noise.

These results offer new insights into the practical use of hybrid UA-NLA under realistic conditions, both for one-way communication and for end-to-end transmission over quantum repeater chains [35–37].

## VI. ACKNOWLEDGEMENT

SNS is grateful to M. Winnel for helpful discussions on Kraus operators and key rates. SNS was supported by the Sydney Quantum Academy, Sydney, NSW, Australia. This work was partially supported by the Australian Research Council Centre of Excellence for Quantum Computation and Communication Technology (Project No.CE110001027).

## Appendix A: Unitary Averaging in a nutshell

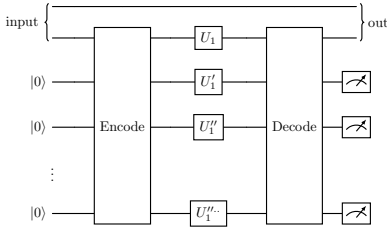


Figure 7: A passive unitary averaging scheme utilises a beam splitter network for redundant encoding over  $n$  modes. One mode of a two-mode state is evenly distributed across  $n$  transmission modes. Each mode undergoes independent single-mode unitary noise. The decoding network reverses the encoding process, and upon heralding  $n - 1$  error modes in the vacuum state,

the output state exhibits reduced noise.

We begin by reviewing previous work on Gaussian systems, in which the impact of UA on a continuous-variable (CV) system is modelled using a two-mode squeezed vacuum state, as described in [12]. In this model, a passive beam splitter encoding network is employed to place the input state into an equal superposition of  $n$  spatial modes. Each of these modes undergo independent transformations, previously simply transmission though phase noise, we are now considering arbitrary linear optical unitary transformations. The decoding network then inverts the encoding such that each superposition should constructively interfere in the top most modes. The remaining ‘error modes’ are then heralded in the vacuum state, such that the heralded output state exhibits suppressed

noise. The behaviour is characterised by the resulting output squeezing, purity, and entanglement. The two-mode squeezed vacuum state was chosen for characterising the system because it can effectively represent various input states through projective measurement. Fig. 7 illustrates the circuit discussed in Ref. [12]. Below, we provide a brief summary of the corresponding results.

The output state from the the protocol is,

$$|\psi_{\text{out}}\rangle = \frac{1}{\mathbf{N}} (\cosh r)^{-1} \sum_N (-1)^N [e^{i\phi_\beta} \tanh r']^N |N, N\rangle = \hat{S}(\chi') |0\rangle |0\rangle \quad (\text{A1})$$

where  $\chi' = r' e^{i\phi_\beta}$  and the phase terms  $\phi_j$  vary randomly and independently around some mean value. We define  $\alpha e^{i\phi_\beta} = \frac{e^{i\phi_1} + e^{i\phi_2} + \dots + e^{i\phi_n}}{n}$  and  $\tanh r' = \alpha \tanh r$  with normalisation constant  $\mathbf{N} = \frac{\cosh r'}{\cosh r}$  and probability of success  $P = |\mathbf{N}|^2$ .

In the covariance matrix form we have,

$$\Sigma_{\text{out}(4 \times 4)} = \left\langle \begin{pmatrix} A & C \\ C^T & B \end{pmatrix} \right\rangle \quad (\text{A2})$$

where,

$$A = B = \begin{pmatrix} \frac{1+\tanh r'^2}{1-\tanh r'^2} & 0 \\ 0 & \frac{1+\tanh r'^2}{1-\tanh r'^2} \end{pmatrix} \quad (\text{A3})$$

$$C = \begin{pmatrix} -\frac{2\tanh r'}{1-\tanh r'^2} \cos(\phi_\beta) & \mathcal{C} \\ \mathcal{C} & \frac{2\tanh r'}{1-\tanh r'^2} \cos(\phi_\beta) \end{pmatrix} \quad (\text{A4})$$

$$\mathcal{C} = 2(\cosh r')^{-2} \sum_N (N+1)(\tanh r')^{2N+1} \sin(\phi_\beta) \quad (\text{A5})$$

and  $C = C^T$ . The analytical expression for the unitary averaging model in the low noise limit assuming the individual random phases  $\phi_j$  are independent Gaussian parameters with mean zero and variance  $v$  can be approximated as

$$\langle \tanh r' \rangle \approx \left(1 - \left(\frac{v}{2} - \frac{v}{2n}\right)\right) \tanh r \quad (\text{A6})$$

$$\langle \cos(\phi_\beta) \rangle \approx \cos\left(\sqrt{\frac{v}{n}}\right) \quad (\text{A7})$$

where we have assumed  $v \ll 1$  and

$$\left\langle \frac{2\tanh r'}{1-\tanh r'^2} \cos(\phi_\beta) \right\rangle \approx \frac{2\langle \tanh r' \rangle}{1-\langle \tanh r' \rangle^2} \langle \cos(\phi_\beta) \rangle \quad (\text{A8})$$

$$\langle \mathcal{C} \rangle \approx 0 \quad (\text{A9})$$

In summary, we introduced a unitary averaging (UA) scheme with continuous variables that incorporates vacuum detection [12]. This approach effectively mitigates the impact of phase noise within the channel. Interestingly, our results demonstrated more than an order of magnitude reduction in noise, along with improvements in squeezing, purity, and entanglement levels in practical systems. Moving forward, we will extend the UA scheme to a multi-mode channel with arbitrary interferometer noise. In the following section, we begin by examining the two-mode channel.

## Appendix B: BRIEF REVIEW OF THE PHASE-SPACE FORMALISM

As outlined in the main text, in order to analyse the continuous-variable quantum key distribution protocol, we employ the phase-space formalism [1, 22, 25, 26, 28]. The following subsections are intended merely as a concise review of the relevant formalism to support the results presented in the main text.

### 1. Mode and quadrature operators

We consider bosonic systems composed of  $N$  harmonic oscillators, each associated with annihilation and creation operators  $\hat{a}_j$  and  $\hat{a}_j^\dagger$ , where  $j = 1, \dots, N$ . The operators  $\hat{a}_j$  will also be referred to as mode operators. Throughout, we set  $\hbar = 2$  and adopt the canonical commutation relations.

$$[\hat{a}_j, \hat{a}_k] = [\hat{a}_j^\dagger, \hat{a}_k^\dagger] = 0, \quad (B1)$$

$$[\hat{a}_j, \hat{a}_k^\dagger] = \delta_{jk} \quad (B2)$$

We define Hermitian position- and momentum-like operators for each mode

$$\hat{x}_j = (\hat{a}_j + \hat{a}_j^\dagger) \quad (B3)$$

$$\hat{p}_j = i(\hat{a}_j^\dagger - \hat{a}_j) \quad (B4)$$

with the canonical commutator

$$[\hat{x}_j, \hat{p}_k] = 2i\delta_{jk} \quad (B5)$$

Following the convention in quantum optics, we also refer to  $\hat{x}_j$  and  $\hat{p}_j$  as quadrature operators. For convenience, we collect the  $2N$  quadrature operators corresponding to the  $N$  modes into a single column vector, which we define as

$$\hat{r} = \begin{pmatrix} \hat{x}_1 \\ \hat{p}_1 \\ \vdots \\ \hat{x}_N \\ \hat{p}_N \end{pmatrix} \quad (B6)$$

The canonical commutation relations can then be written

$$[\hat{r}_j, \hat{r}_k] = \Omega_{jk} \quad (B7)$$

where  $\Omega$  is the symplectic matrix defined by

$$\Omega = \bigoplus_{j=1}^{2N} \begin{pmatrix} 0 & 1 \\ -1 & 0 \end{pmatrix} = \mathbb{I}_N \otimes \begin{pmatrix} 0 & 1 \\ -1 & 0 \end{pmatrix} \quad (B8)$$

where  $\mathbb{I}_N$  is the  $N \times N$  identity matrix.

## 2. Covariance Matrices

Given a quantum state  $\rho$  of an  $N$ -mode system, the corresponding covariance matrix  $V$  has elements

$$V_{jk} = \langle \{\hat{r}_j, \hat{r}_k\} \rangle - \langle \hat{r}_j \rangle \langle \hat{r}_k \rangle \quad (B9)$$

where  $\{\cdot, \cdot\}$  denotes the anticommutator and  $\langle \hat{A} \rangle$  is the expectation value. For a valid density matrix  $\rho$ , the covariance matrix  $V$  is real, symmetric, and positive definite ( $V > 0$ ), and it satisfies

$$V + i\Omega \geq 0 \quad (B10)$$

Note that the diagonal elements of  $V$  represent the variances of the quadrature operators, whereas the non-zero off-diagonal elements correspond to the correlations between different quadratures.

## Appendix C: CALCULATION OF THE VARIOUS PROTOCOL

As discussed in the main text, we conduct the security analysis by leveraging the optimality of Gaussian attacks [20]. When Alice and Bob share a non-Gaussian state  $\rho$ , a lower bound on the exact SKR can be obtained by considering a corresponding Gaussian protocol in which they share a Gaussian state  $\rho_G$  possessing the same CM as  $\rho$ . In this Appendix, we derive the CM for the protocols presented in the main text. To achieve this, we employ the input-output formalism along with the Kraus operator representation of quantum states.

### 1. KRAUS OPERATOR REPRESENTATION

In a lossy thermal-noise channel, the input state  $\rho_0$  interacts with a thermal state  $\rho_{th}$  through a beam splitter with transmissivity  $\eta$ . After the interaction, the environment is traced out, resulting in the channel's output state. A possible Kraus operator representation can be obtained by decomposing the lossy thermal-noise channel into a pure-loss channel with transmissivity  $\tau = \eta/G$ ,

followed by a quantum-limited amplifier with gain  $G = 1 + (1 - \eta)\bar{n} = \frac{\eta\epsilon}{2} + 1$ , where  $\eta$  represents the pure loss and  $\epsilon$  denotes the excess noise [38]. This decomposition yields the following Kraus representation for the lossy thermal-noise channel:

$$\mathbb{W}(\rho_0) = \sum_{k,l}^{\infty} \hat{B}_k \hat{A}_l \rho_0 \hat{A}_l^\dagger \hat{B}_k^\dagger \quad (\text{C1})$$

where  $\hat{A}_l$  are the Kraus operators of the pure loss channel, while  $\hat{B}_k$  are the Kraus operators of the quantum limited amplifier [38] given by

$$\hat{A}_l = \sqrt{\frac{(1 - \tau)^l}{l!}} \tau^{\hat{n}/2} \hat{a}^l \quad (\text{C2})$$

$$\hat{B}_k = \sqrt{\frac{1}{k!} \frac{1}{G} \left(\frac{G-1}{G}\right)^k} \hat{a}^k G^{-\hat{n}/2} \quad (\text{C3})$$

where  $\hat{n}$  is the number operator.  $\hat{a}$  and  $\hat{a}^\dagger$  are annihilation and creation operator respectively.

## 2. CALCULATION OF THE CM WITH PHASE NOISE

In this subsection, we detail the calculation of a scenario detailed in section III and in fig.1. The  $\rho_0$  of input TMSV is,

$$|\psi_0\rangle = (\cosh r)^{-1} \sum_{n=0}^{\infty} (-\tanh r)^n |n, n\rangle \quad (\text{C4})$$

$$\rho_0 = (\cosh r)^{-2} \sum_{n=0}^{\infty} \sum_{m=0}^{\infty} (\tanh r)^{n+m} |n, n\rangle \langle m, m| \quad (\text{C5})$$

The phase shift noise defined as

$$R(\phi) = \exp(i\phi\hat{n}), \hat{n} = \hat{a}^\dagger \hat{a} \quad (\text{C6})$$

The noise we consider is fluctuations in phase shifter (PS) parameters, which are modelled as independent Gaussian noise on each mode drawn from the same distribution. With the application of  $R_2(\phi)$  on second mode of the EQ.C5,

$$\rho_{\text{PS}} = R_2(\phi) (\cosh r)^{-2} \sum_{n=0}^{\infty} \sum_{m=0}^{\infty} (\tanh r)^{n+m} |n, n\rangle \langle m, m| R_2(\phi)^\dagger \quad (\text{C7})$$

$$= (\cosh r)^{-2} \sum_{n=0}^{\infty} \sum_{m=0}^{\infty} (\tanh r)^{n+m} \exp(i\phi\hat{a}_2^\dagger \hat{a}_2) |n, n\rangle \langle m, m| \exp(-i\phi\hat{a}_2 \hat{a}_2^\dagger) \quad (\text{C8})$$

With the thermal loss channel, using Eq.C1 in Eq.C8

$$\mathbb{W}(\rho_{\text{PS}}) = \sum_{k,l}^{\infty} \hat{B}_k \hat{A}_l \rho_{\text{PS}} \hat{A}_l^\dagger \hat{B}_k^\dagger \quad (\text{C9})$$

Finally, we compute the covariance matrix (CM) associated with the state eq.C9.

$$\mathbb{A}_{\text{PS}} = \text{Tr}(\rho_{\text{PS}} q_A^2) \quad (\text{C10})$$

$$\mathbb{B}_{\text{PS}} = \text{Tr}(\rho_{\text{PS}} q_B^2) \quad (\text{C11})$$

$$\mathbb{C}_{\text{PS}} = \text{Tr}(\rho_{\text{PS}} q_A q_B) \quad (\text{C12})$$

Accordingly, the CM is written

$$\Sigma_{AB}^{(\text{PS})} = \begin{pmatrix} \mathbb{A}_{\text{PS}} \mathbf{I}_2 & \mathbb{C}_{\text{PS}} \sigma_2 \\ \mathbb{C}_{\text{PS}} \sigma_2 & \mathbb{B}_{\text{PS}} \mathbf{I}_2 \end{pmatrix} \quad (\text{C13})$$

The CM (C13) in terms of  $\eta$  and  $\epsilon$ ,

$$\Sigma_{AB}^{(\text{PS})} \equiv \begin{pmatrix} \cosh 2r \mathbf{I}_2 & \sqrt{\eta} \sinh 2r \cos \phi \sigma_2 \\ \sqrt{\eta} \sinh 2r \cos \phi \sigma_2 & \eta(\cosh 2r + \frac{1-\eta}{\eta} + \epsilon) \mathbf{I}_2 \end{pmatrix} \quad (\text{C14})$$

where  $r$  is the squeezing factor and  $\eta$  is the pure loss.

## 3. CALCULATION OF CM WITH UNITARY AVERAGING

In this subsection, we detail the calculation of results explained in section III and in fig.2.

The input state reads,

$$\psi_1 = |\psi_0\rangle |0\rangle \quad (\text{C15})$$

$$= (\cosh r)^{-1} \sum_{n=0}^{\infty} (-\tanh r)^n |n, n\rangle_{a1,b1} |0\rangle_{a2} \quad (\text{C16})$$

$$\rho_1 = (\cosh r)^{-2} \sum_{n=0}^{\infty} \sum_{m=0}^{\infty} (\tanh r)^{n+m} |n, n, 0\rangle_{a1,b1,a2} \langle m, m, 0|_{a1,b1,a2} \quad (\text{C17})$$

$$= (\cosh r)^{-2} \sum_{n=0}^{\infty} \sum_{m=0}^{\infty} (\tanh r)^{n+m} (\hat{a}_1^\dagger)^n (\hat{b}_1^\dagger)^m |0, 0, 0\rangle_{a1,b1,a2} \langle 0, 0, 0|_{a1,b1,a2} \quad (\text{C18})$$

The unitary transformation with loss and excess noise

$$\hat{\mathbf{U}} = \hat{B}_{b1a2}^{(50:50)} R(\hat{\phi}_{b1}) \mathbb{W}_{b1} R(\hat{\phi}_{a2}) \mathbb{W}_{a2} \hat{B}_{b1a2}^{(50:50)\dagger} \quad (\text{C19})$$

where  $\hat{B}_{b1a2}^{(50:50)}$  is the 50 : 50 beamsplitter between modes  $b1$  and  $a2$ .  $\mathbb{W}_{b1}$  and  $\mathbb{W}_{a2}$  are thermal loss channel on modes  $b1$  and  $a2$  respectively. Similarly,  $R(\hat{\phi}_{b1})$  and  $R(\hat{\phi}_{a2})$  are phase shifters on mode  $b1$  and  $a2$  respectively. As  $\mathbb{W}_{b1}$  and  $\mathbb{W}_{a2}$  commute with beamsplitters and phase shifters, we can consider applying the the thermal loss channel after the decoding step.

Now, we define UA transformation as

$$\hat{U}_{UA} = \hat{B}_{b1a2}^{(50:50)} R(\hat{\phi}_{b1}) R(\hat{\phi}_{a2}) \hat{B}_{b1a2}^{(50:50)\dagger} \quad (C20)$$

$$= \exp\left(\frac{\pi}{4}(\hat{b1}^\dagger \hat{a2} - \hat{b1} \hat{a2}^\dagger)\right) \exp\left(i\phi_{b1} \hat{b1}^\dagger \hat{b1}\right) \\ \exp\left(i\phi_{a2} \hat{a2}^\dagger \hat{a2}\right) \exp\left(\frac{\pi}{4}(\hat{b1} \hat{a2}^\dagger - \hat{b1}^\dagger \hat{a2})\right) \quad (C21)$$

In the Heisenberg picture, the annihilation operators are transformed via the linear unitary Bogoliubov transformation as

$$\begin{pmatrix} \hat{b1}' \\ \hat{a2}' \end{pmatrix} \rightarrow \frac{1}{2} \begin{pmatrix} 1 & 1 \\ -1 & 1 \end{pmatrix} \begin{pmatrix} e^{i\phi_{b1}} & 0 \\ 0 & e^{i\phi_{a2}} \end{pmatrix} \begin{pmatrix} 1 & -1 \\ 1 & 1 \end{pmatrix} \begin{pmatrix} \hat{b1} \\ \hat{a2} \end{pmatrix} \quad (C22)$$

$$\rightarrow \frac{1}{2} \begin{pmatrix} e^{i\phi_{b1}} + e^{i\phi_{a2}} & e^{i\phi_{a2}} - e^{i\phi_{b1}} \\ e^{i\phi_{a2}} - e^{i\phi_{b1}} & e^{i\phi_{b1}} + e^{i\phi_{a2}} \end{pmatrix} \begin{pmatrix} \hat{b1} \\ \hat{a2} \end{pmatrix} \quad (C23)$$

$$\hat{b1}' \rightarrow \frac{1}{2} ((e^{i\phi_{b1}} + e^{i\phi_{a2}}) \hat{b1} + (e^{i\phi_{a2}} - e^{i\phi_{b1}}) \hat{a2}) \quad (C24)$$

$$\hat{a2}' \rightarrow \frac{1}{2} ((e^{i\phi_{a2}} - e^{i\phi_{b1}}) \hat{b1} + (e^{i\phi_{b1}} + e^{i\phi_{a2}}) \hat{a2}) \quad (C25)$$

Applying  $\hat{U}_{UA}$  to the Eq.C18

$$\rho_{UA} \rightarrow \hat{U}_{UA} \rho_1 \hat{U}_{UA}^\dagger \quad (C26)$$

$$\rho_{UA} = (\cosh r)^{-2} \sum_{n=0}^{\infty} \sum_{m=0}^{\infty} (\tanh r)^{n+m} \hat{U}_{UA} (\hat{a}_1^\dagger)^n (\hat{b}_1^\dagger)^m \\ |0,0,0\rangle_{a1,b1,a2} \langle 0,0,0|_{a1,b1,a2} (\hat{a}_1^\dagger)^m (\hat{b}_1^\dagger)^m \hat{U}_{UA}^\dagger \quad (C27)$$

$$= (\cosh r)^{-2} \sum_{n=0}^{\infty} \sum_{m=0}^{\infty} (\tanh r)^{n+m} (\hat{a}_1^\dagger)^n (\hat{b}_1'^\dagger)^m \\ |0,0,0\rangle_{a1,b1,a2} \langle 0,0,0|_{a1,b1,a2} (\hat{a}_1^\dagger)^m (\hat{b}_1'^\dagger)^m \hat{U}_{UA}^\dagger \quad (C28)$$

$$= (\cosh r)^{-2} \sum_{n=0}^{\infty} \sum_{m=0}^{\infty} (\tanh r)^{n+m} (\hat{a}_1^\dagger)^n \\ \left(\frac{1}{2} ((e^{i\phi_{b1}} + e^{i\phi_{a2}}) \hat{b1} + (e^{i\phi_{a2}} - e^{i\phi_{b1}}) \hat{a2})\right)^n \\ |0,0,0\rangle_{a1,b1,a2} \langle 0,0,0|_{a1,b1,a2} (\hat{a}_1^\dagger)^m \\ \left(\frac{1}{2} ((e^{i\phi_{b1}} + e^{i\phi_{a2}}) \hat{b1} + (e^{i\phi_{a2}} - e^{i\phi_{b1}}) \hat{a2})\right)^m \quad (C29)$$

With the thermal loss channel, exploiting Eq.C1 in

Eq.C29

$$\mathbb{W}(\rho_{UA}) = \sum_{kb1,lb1}^{\infty} \sum_{ka2,la2}^{\infty} \hat{B}_{kb1} \hat{A}_{lb1} \hat{B}_{ka2} \hat{A}_{la2} \\ \rho_{UA} \hat{A}_{la2}^\dagger \hat{B}_{ka2}^\dagger \hat{A}_{lb1}^\dagger \hat{B}_{kb1}^\dagger \quad (C30)$$

$$= (\cosh r)^{-2} \sum_{n=0}^{\infty} \sum_{m=0}^{\infty} \sum_{kb1,lb1}^{\infty} \sum_{ka2,la2}^{\infty} \\ \hat{B}_{kb1} \hat{A}_{lb1} \hat{B}_{ka2} \hat{A}_{la2} (\tanh r)^{n+m} (\hat{a}_1^\dagger)^n \\ \left(\frac{1}{2} ((e^{i\phi_{b1}} + e^{i\phi_{a2}}) \hat{b1} + (e^{i\phi_{a2}} - e^{i\phi_{b1}}) \hat{a2})\right)^n \\ |0,0,0\rangle_{a1,b1,a2} \langle 0,0,0|_{a1,b1,a2} (\hat{a}_1^\dagger)^m \\ \left(\frac{1}{2} ((e^{i\phi_{b1}} + e^{i\phi_{a2}}) \hat{b1} + (e^{i\phi_{a2}} - e^{i\phi_{b1}}) \hat{a2})\right)^m \\ \hat{A}_{la2}^\dagger \hat{B}_{ka2}^\dagger \hat{A}_{lb1}^\dagger \hat{B}_{kb1}^\dagger \quad (C31)$$

After applying the vacuum projection operator on mode  $a3$ , the normalised output state is

$$\rho'_{UA} = \frac{(\mathbf{I}_{a1} \otimes \mathbf{I}_{b1} \otimes \langle 0|) \mathbb{W}(\rho_{UA}) (\mathbf{I}_{a1} \otimes \mathbf{I}_{b1} \otimes |0\rangle)}{\text{Tr}((\mathbf{I}_{a1} \otimes \mathbf{I}_{b1} \otimes \langle 0|) \mathbb{W}(\rho_{UA}))} \quad (C32)$$

Normalisation constant represents the success probability of the vacuum detection.

Finally, we compute the CM associated with the state (C41).

$$\mathbb{A}_{UA} = \text{Tr}(\rho'_{UA} q_{a1}^2) \quad (C33)$$

$$\mathbb{B}_{UA} = \text{Tr}(\rho'_{UA} q_{b1}^2) \quad (C34)$$

$$\mathbb{C}_{UA} = \text{Tr}(\rho'_{UA} q_{a1} q_{b1}) \quad (C35)$$

Accordingly, the CM is written

$$\Sigma_{a1b1}^{(UA)} = \begin{pmatrix} \mathbb{A}_{UA} \mathbf{I}_2 & \mathbb{C}_{UA} \sigma_2 \\ \mathbb{C}_{UA} \sigma_2 & \mathbb{B}_{UA} \mathbf{I}_2 \end{pmatrix} \quad (C36)$$

where

$$\mathbf{Z} = \left(\frac{e^{i\phi_{b1}} + e^{i\phi_{a2}}}{2}\right); \phi_j \sim \mathcal{N}(0, \sigma^2) \quad (C37)$$

$$\mathbb{A}_{UA} \equiv \cosh 2r \sqrt{\left(\text{Re}(\mathbf{Z})\right)^2 + \left(\text{Im}(\mathbf{Z})\right)^2} \quad (C38)$$

$$\mathbb{B}_{UA} \equiv \eta \left(\mathbb{A}_{UA} + \frac{1-\eta}{\eta} + \epsilon\right) \quad (C39)$$

$$\mathbb{C}_{UA} \equiv \sqrt{\eta} \sinh 2r \sqrt{\left(\text{Re}(\mathbf{Z})\right)^2 + \left(\text{Im}(\mathbf{Z})\right)^2} \\ \cos \left( \arctan \frac{\text{Im}(\mathbf{Z})}{\text{Re}(\mathbf{Z})} \right) \quad (C40)$$

where  $\text{Re}(\mathbf{Z})$  and  $\text{Im}(\mathbf{Z})$  is the real and imaginary part of  $\mathbf{Z}$ .

#### 4. EMPLOYING QUANTUM SCISSOR AND UNITARY AVERAGING

Alice prepares three modes ( $a1, a2, a3$ ). She applies an encoding beamsplitter between modes ( $a2$ ) and ( $a3$ ) and then sends the encoded modes to Charlie's station. Likewise, Bob prepares three modes ( $b1, b2, b3$ ), applies an encoding beamsplitter between ( $b1$ ) and ( $b3$ ), and forwards the encoded modes to Charlie. Charlie performs vacuum post-selection on modes ( $a3$ ) and ( $b3$ ), then interferes modes ( $a2$ ) and ( $b1$ ) and measures the result with photon-number-resolving detectors.

From subsection C3, following the vacuum detection on mode ( $a3$ ), Alice's unitary-averaged state is given by

$$\rho_A' = \frac{(\mathbf{I}_{a1} \otimes \mathbf{I}_{a2} \otimes \langle 0 |) \mathbb{W}(\rho_A) (\mathbf{I}_{a1} \otimes \mathbf{I}_{a2} \otimes | 0 \rangle)}{\text{Tr}((\mathbf{I}_{a1} \otimes \mathbf{I}_{a2} \otimes \langle 0 |) \mathbb{W}(\rho_{UA}))} \quad (\text{C41})$$

Bob prepares three modes in the Fock states  $|1\rangle_{b1}$ ,  $|0\rangle_{b2}$ , and  $|1\rangle_{b3}$  respectively. He mixes them at a beam splitter with transmissivity  $\mathbb{T} = \frac{1}{1+g^2}$ . It fixes the gain associated with the NLA; that for low-amplitude coherent signals reads  $g = \sqrt{\frac{1-\mathbb{T}}{\mathbb{T}}}$

$$|\psi\rangle_B = |1\rangle_{b1} |0\rangle_{b2} |0\rangle_{b3} \quad (\text{C42})$$

$$\rho_B = |1\rangle_{b1} \langle 0 |_{b2} \langle 0 |_{b3} \langle 1 |_{b1} \langle 0 |_{b2} \langle 0 |_{b3} \quad (\text{C43})$$

The beamsplitter with transmissivity  $\mathbb{T} = \frac{1}{1+g^2}$  changes the modes  $b1$  and  $b2$  as

$$\begin{pmatrix} \hat{b1}' \\ \hat{b2}' \end{pmatrix} \rightarrow \begin{pmatrix} \sqrt{\mathbb{T}} & \sqrt{1-\mathbb{T}} \\ -\sqrt{1-\mathbb{T}} & \sqrt{\mathbb{T}} \end{pmatrix} \begin{pmatrix} \hat{b1} \\ \hat{b2} \end{pmatrix} \quad (\text{C44})$$

Applying Eq.C44 to the state (C43),

$$\begin{aligned} \rho_B = & \left( \sqrt{\mathbb{T}} \hat{b1}^\dagger + \sqrt{1-\mathbb{T}} \hat{b2}^\dagger \right) |0\rangle_{b1} |0\rangle_{b2} |0\rangle_{b3} \\ & \langle 0 |_{b1} \langle 0 |_{b2} \langle 0 |_{b3} \left( \sqrt{\mathbb{T}} \hat{b1}^\dagger + \sqrt{1-\mathbb{T}} \hat{b2}^\dagger \right) \end{aligned} \quad (\text{C45})$$

After UA, using Eq.C21,

$$\hat{b1}' \rightarrow \frac{1}{2} \left( (e^{i\phi_{b1}} + e^{i\phi_{b3}}) \hat{b1} + (e^{i\phi_{b3}} - e^{i\phi_{b1}}) \hat{b3} \right) \quad (\text{C46})$$

$$\begin{aligned} \rho_B = & \left( \sqrt{\mathbb{T}} \hat{b1}'^\dagger + \sqrt{1-\mathbb{T}} \hat{b2}^\dagger \right) |0\rangle_{b1} |0\rangle_{b2} |0\rangle_{b3} \\ & \langle 0 |_{b1} \langle 0 |_{b2} \langle 0 |_{b3} \left( \sqrt{\mathbb{T}} \hat{b1}'^\dagger + \sqrt{1-\mathbb{T}} \hat{b2}^\dagger \right) \end{aligned} \quad (\text{C47})$$

$$\begin{aligned} = & \left( \sqrt{\mathbb{T}} \left( \frac{1}{2} \left( (e^{i\phi_{b1}} + e^{i\phi_{b3}}) \hat{b1} + (e^{i\phi_{b3}} - e^{i\phi_{b1}}) \hat{b3} \right) \right. \right. \\ & \left. \left. + \sqrt{1-\mathbb{T}} \hat{b2}^\dagger \right) |0\rangle_{b1} |0\rangle_{b2} |0\rangle_{b3} \langle 0 |_{b1} \langle 0 |_{b2} \langle 0 |_{b3} \right. \\ & \left. \left( \sqrt{\mathbb{T}} \left( \frac{1}{2} \left( (e^{i\phi_{b1}} + e^{i\phi_{b3}}) \hat{b1} + (e^{i\phi_{b3}} - e^{i\phi_{b1}}) \hat{b3} \right) \right. \right. \\ & \left. \left. + \sqrt{1-\mathbb{T}} \hat{b2}^\dagger \right) \right) \end{aligned} \quad (\text{C48})$$

With the thermal loss channel (C1),

$$\begin{aligned} \mathbb{W}(\rho_B) = & \sum_{kb1, lb1}^{\infty} \sum_{kb3, lb3}^{\infty} \hat{B}_{kb1} \hat{A}_{lb1} \hat{B}_{kb3} \hat{A}_{lb3} \\ & \rho_B \hat{A}_{lb3}^\dagger \hat{B}_{kb3}^\dagger \hat{A}_{lb1}^\dagger \hat{B}_{kb1}^\dagger \end{aligned} \quad (\text{C49})$$

$$\begin{aligned} = & \sum_{kb1, lb1}^{\infty} \sum_{kb3, lb3}^{\infty} \hat{B}_{kb1} \hat{A}_{lb1} \hat{B}_{kb3} \hat{A}_{lb3} \\ & \left( \sqrt{\mathbb{T}} \left( \frac{1}{2} \left( (e^{i\phi_{b1}} + e^{i\phi_{b3}}) \hat{b1} + (e^{i\phi_{b3}} - e^{i\phi_{b1}}) \hat{b3} \right) \right. \right. \\ & \left. \left. + \sqrt{1-\mathbb{T}} \hat{b2}^\dagger \right) |0\rangle_{b1} |0\rangle_{b2} |0\rangle_{b3} \langle 0 |_{b1} \langle 0 |_{b2} \langle 0 |_{b3} \right. \\ & \left. \left( \sqrt{\mathbb{T}} \left( \frac{1}{2} \left( (e^{i\phi_{b1}} + e^{i\phi_{b3}}) \hat{b1} + (e^{i\phi_{b3}} - e^{i\phi_{b1}}) \hat{b3} \right) \right. \right. \\ & \left. \left. + \sqrt{1-\mathbb{T}} \hat{b2}^\dagger \right) \right) \hat{A}_{lb3}^\dagger \hat{B}_{kb3}^\dagger \hat{A}_{lb1}^\dagger \hat{B}_{kb1}^\dagger \end{aligned} \quad (\text{C50})$$

After applying the vacuum projection operator on mode  $b3$ , the normalised output state is

$$\rho_B' = \frac{(\mathbf{I}_{b1} \otimes \mathbf{I}_{b2} \otimes \langle 0 |) \mathbb{W}(\rho_B) (\mathbf{I}_{b1} \otimes \mathbf{I}_{b2} \otimes | 0 \rangle)}{\text{Tr}((\mathbf{I}_{b1} \otimes \mathbf{I}_{b2} \otimes \langle 0 |) \mathbb{W}(\rho_B))} \quad (\text{C51})$$

Normalisation constant represents the success probability of the vacuum detection of Bob's mode at Charlie's station.

Now Charlie connected modes  $a2$  and  $b1$  via a balanced beamsplitter and performs photon number resolving detection.

$$\rho_{AB} = \hat{B}_{a2b1}^{(50:50)} \left( \rho_A(a1, a2) \otimes \rho_B(b1, b2) \right) \hat{B}_{a2b1}^{(50:50)\dagger} \quad (\text{C52})$$

$$\rho_{AB}' = \frac{(\mathbf{I}_{a1} \otimes \langle 0 | \otimes \langle 1 | \otimes \mathbf{I}_{b2}) \rho_{AB} (\mathbf{I}_{a1} \otimes | 0 \rangle \otimes | 1 \rangle \otimes \mathbf{I}_{b2})}{\text{Tr}((\mathbf{I}_{a1} \otimes \langle 0 | \otimes \langle 1 | \otimes \mathbf{I}_{b2}) \rho_{AB})} \quad (\text{C53})$$

The global success probability of the QS-based NLA is  $P_{QS} = 2 \text{Tr}((\mathbf{I}_{a1} \otimes \langle 0 | \otimes \langle 1 | \otimes \mathbf{I}_{b2}) \rho_{AB})$ .

Finally, we compute the CM associated with the state (C51).

$$\mathbb{A}_{AB} = \text{Tr}(\rho_{AB}' q_{a1}^2) \quad (\text{C54})$$

$$\mathbb{B}_{AB} = \text{Tr}(\rho_{AB}' q_{b2}^2) \quad (\text{C55})$$

$$\mathbb{C}_{AB} = \text{Tr}(\rho_{AB}' q_{a1} q_{b2}) \quad (\text{C56})$$

Accordingly, the CM is written

$$\Sigma_{a1b2}^{(AB)} = \begin{pmatrix} \mathbb{A}_{AB} \mathbf{I}_2 & \mathbb{C}_{AB} \sigma_2 \\ \mathbb{C}_{AB} \sigma_2 & \mathbb{B}_{AB} \mathbf{I}_2 \end{pmatrix} \quad (\text{C57})$$

---

[1] C. Weedbrook, S. Pirandola, R. García-Patrón, N. J. Cerf, T. C. Ralph, J. H. Shapiro, and S. Lloyd, Gaussian quantum information, *Reviews of Modern Physics* **84**, 621 (2012).

[2] T. C. Ralph, Continuous variable quantum cryptography, *Physical Review A* **61**, 010303 (1999).

[3] F. Grosshans and P. Grangier, Continuous variable quantum cryptography using coherent states, *Physical review letters* **88**, 057902 (2002).

[4] C. Weedbrook, A. M. Lance, W. P. Bowen, T. Symul, . f. T. C. Ralph, and P. K. Lam, Quantum cryptography without switching, *Physical review letters* **93**, 170504 (2004).

[5] F. Grosshans, Collective attacks and unconditional security in continuous variable quantum key distribution, *Physical review letters* **94**, 020504 (2005).

[6] F. Laudenbach, C. Pacher, C.-H. F. Fung, A. Poppe, M. Peev, B. Schrenk, M. Hentschel, P. Walther, and H. Hübel, Continuous-variable quantum key distribution with gaussian modulation—the theory of practical implementations, *Advanced Quantum Technologies* **1**, 1800011 (2018).

[7] F. Grosshans, N. J. Cerf, J. Wenger, R. Tualle-Brouri, and P. Grangier, Virtual entanglement and reconciliation protocols for quantum cryptography with continuous variables, *arXiv preprint quant-ph/0306141* (2003).

[8] F. Grosshans and P. Grangier, Reverse reconciliation protocols for quantum cryptography with continuous variables, *arXiv preprint quant-ph/0204127* (2002).

[9] J. Lodewyck, M. Bloch, R. García-Patrón, S. Fossier, E. Karpov, E. Diamanti, T. Debuisschert, N. J. Cerf, R. Tualle-Brouri, S. W. McLaughlin, *et al.*, Quantum key distribution over 25 km with an all-fiber continuous-variable system, *Physical Review A—Atomic, Molecular, and Optical Physics* **76**, 042305 (2007).

[10] S. P. Kish, P. Gleeson, P. K. Lam, and S. M. Assad, Comparison of discrete variable and continuous variable quantum key distribution protocols with phase noise in the thermal-loss channel, *Quantum* **8**, 1382 (2024).

[11] R. J. Marshman, A. P. Lund, P. P. Rohde, and T. C. Ralph, Passive quantum error correction of linear optics networks through error averaging, *Physical Review A* **97**, 022324 (2018).

[12] S. N. Swain, R. J. Marshman, P. P. Rohde, A. P. Lund, A. S. Solntsev, and T. C. Ralph, Improving continuous-variable quantum channels with unitary averaging, *Physical Review A* **110**, 032622 (2024).

[13] T. Ralph and A. Lund, Nondeterministic noiseless linear amplification of quantum systems, in *AIP Conference Proceedings*, Vol. 1110 (AIP Publishing, 2009) pp. 155–160.

[14] T. Ralph, Quantum error correction of continuous-variable states against gaussian noise, *Physical Review A—Atomic, Molecular, and Optical Physics* **84**, 022339 (2011).

[15] G.-Y. Xiang, T. C. Ralph, A. P. Lund, N. Walk, and G. J. Pryde, Heralded noiseless linear amplification and distillation of entanglement, *Nature Photonics* **4**, 316 (2010).

[16] H. Adnane, B. Teklu, and M. G. Paris, Quantum phase communication channels assisted by non-deterministic noiseless amplifiers, *Journal of the Optical Society of America B* **36**, 2938 (2019).

[17] R. Blandino, A. Leverrier, M. Barbieri, J. Etesse, P. Grangier, and R. Tualle-Brouri, Improving the maximum transmission distance of continuous-variable quantum key distribution using a noiseless amplifier, *Physical Review A—Atomic, Molecular, and Optical Physics* **86**, 012327 (2012).

[18] T. C. Ralph and A. Lund, Nondeterministic noiseless linear amplification of quantum systems, *arXiv preprint arXiv:0809.0326* (2008).

[19] M. Ghalai, C. Ottaviani, R. Kumar, S. Pirandola, and M. Razavi, Discrete-modulation continuous-variable quantum key distribution enhanced by quantum scissors, *IEEE Journal on Selected Areas in Communications* **38**, 506 (2020).

[20] S. Pirandola, R. Laurenza, C. Ottaviani, and L. Banchi, Fundamental limits of repeaterless quantum communications, *Nature communications* **8**, 15043 (2017).

[21] M. S. Winnel, J. J. Guanzon, N. Hosseini, and T. C. Ralph, Overcoming the repeaterless bound in continuous-variable quantum communication without quantum memories, *arXiv preprint arXiv:2105.03586* (2021).

[22] H.-A. Bachor and T. C. Ralph, *A guide to experiments in quantum optics*, (3rd Edition Wiley, New York, 2019).

[23] X. Li, P. L. Voss, J. E. Sharping, and P. Kumar, Optical-fiber source of polarization-entangled photons in the 1550 nm telecom band, *Physical review letters* **94**, 053601 (2005).

[24] M. V. Larsen, X. Guo, C. R. Breum, J. S. Neergaard-Nielsen, and U. L. Andersen, Fiber-coupled epr-state generation using a single temporally multiplexed squeezed light source, *npj Quantum Information* **5**, 46 (2019).

[25] A. Ferraro, S. Olivares, and M. G. Paris, Gaussian states in continuous variable quantum information, *arXiv preprint quant-ph/0503237* (2005).

[26] A. Serafini, *Quantum continuous variables: a primer of theoretical methods* (CRC press, 2023).

[27] R. García-Patrón and N. J. Cerf, Continuous-variable quantum key distribution protocols over noisy channels, *Physical Review Letters* **102**, 130501 (2009).

[28] S. Olivares, Quantum optics in the phase space: A tutorial on gaussian states, *The European Physical Journal Special Topics* **203**, 3 (2012).

[29] F. Grosshans, G. Van Assche, J. Wenger, R. Brouri, N. J. Cerf, and P. Grangier, Quantum key distribution using gaussian-modulated coherent states, *Nature* **421**, 238 (2003).

[30] S. Pirandola, U. L. Andersen, L. Banchi, M. Berta, D. Bunandar, R. Colbeck, D. Englund, T. Gehring, C. Lupo, C. Ottaviani, *et al.*, Advances in quantum cryptography, *Advances in optics and photonics* **12**, 1012 (2020).

[31] A. S. Holevo, The capacity of the quantum channel with general signal states, *IEEE Transactions on Information Theory* **44**, 269 (2002).

[32] A. Leverrier and P. Grangier, Unconditional security proof of long-distance continuous-variable quantum key distribution with discrete modulation, *Physical review letters* **102**, 180504 (2009).

[33] D. T. Pegg, L. S. Phillips, and S. M. Barnett, Optical

state truncation by projection synthesis, *Physical review letters* **81**, 1604 (1998).

[34] J. J. Guanzon, M. S. Winnel, A. P. Lund, and T. C. Ralph, Ideal quantum teleamplification up to a selected energy cutoff using linear optics, *Physical Review Letters* **128**, 160501 (2022).

[35] J. Dias, M. S. Winnel, N. Hosseinidehaj, and T. C. Ralph, Quantum repeater for continuous-variable entanglement distribution, *Physical Review A* **102**, 052425 (2020).

[36] S. Pirandola, End-to-end capacities of a quantum communication network, *Communications Physics* **2**, 51 (2019).

[37] X. Zhong, W. Wang, L. Qian, and H.-K. Lo, Proof-of-principle experimental demonstration of twin-field quantum key distribution over optical channels with asymmetric losses, *npj Quantum Information* **7**, 8 (2021).

[38] J. S. Ivan, K. K. Sabapathy, and R. Simon, Operator-sum representation for bosonic gaussian channels, *Physical Review A—Atomic, Molecular, and Optical Physics* **84**, 042311 (2011).